Rapid deposition of oxidized biogenic compounds to a temperate forest

Tran B. Nguyen[a,1,2], John D. Crounse[a,1], Alex P. Teng[a], Jason M. St. Clair[a], Fabien Paulot[b,c], Glenn M. Wolfe[d,e], and Paul O. Wennberg[a,f,2]

Divisions of [a]Geological and Planetary Sciences and [f]Engineering and Applied Science, California Institute of Technology, Pasadena, CA 91125; [b]Geophysical Fluid Dynamics Laboratory, National Oceanic and Atmospheric Administration, Princeton, NJ 08540; [c]Atmospheric and Oceanic Sciences, Princeton University, Princeton, NJ 08544; [d]Atmospheric Chemistry and Dynamics Lab, NASA Goddard Space Flight Center, Greenbelt, MD 20771; and [e]Joint Center for Earth Systems Technology, University of Maryland Baltimore County, Baltimore, MD 21250

Edited by Mark H. Thiemens, University of California, San Diego, La Jolla, CA, and approved December 22, 2014 (received for review September 28, 2014)

We report fluxes and dry deposition velocities for 16 atmospheric compounds above a southeastern United States forest, including: hydrogen peroxide (H_2O_2), nitric acid (HNO_3), hydrogen cyanide (HCN), hydroxymethyl hydroperoxide, peroxyacetic acid, organic hydroxy nitrates, and other multifunctional species derived from the oxidation of isoprene and monoterpenes. The data suggest that dry deposition is the dominant daytime sink for small, saturated oxygenates. Greater than 6 wt %C emitted as isoprene by the forest was returned by dry deposition of its oxidized products. Peroxides account for a large fraction of the oxidant flux, possibly eclipsing ozone in more pristine regions. The measured organic nitrates comprise a sizable portion (15%) of the oxidized nitrogen input into the canopy, with HNO_3 making up the balance. We observe that water-soluble compounds (e.g., strong acids and hydroperoxides) deposit with low surface resistance whereas compounds with moderate solubility (e.g., organic nitrates and hydroxycarbonyls) or poor solubility (e.g., HCN) exhibited reduced uptake at the surface of plants. To first order, the relative deposition velocities of water-soluble compounds are constrained by their molecular diffusivity. From resistance modeling, we infer a substantial emission flux of formic acid at the canopy level (~1 nmol $m^{-2}{\cdot}s^{-1}$). GEOS–Chem, a widely used atmospheric chemical transport model, currently underestimates dry deposition for most molecules studied in this work. Reconciling GEOS–Chem deposition velocities with observations resulted in up to a 45% decrease in the simulated surface concentration of trace gases.

biosphere–atmosphere exchange | isoprene | dry deposition | OVOCs | fluxes

Forests are major sources of volatile organic compounds (VOCs), contributing approximately half of the reactive carbon emissions worldwide (1). Emissions of a single compound, isoprene (C_5H_8), contribute approximately a third of the global VOC flux (2). The emitted carbon is transformed in the atmosphere by photolysis and oxidation reactions with the hydroxyl radical (OH), ozone (O_3), or the nitrate radical (NO_3), generating highly oxidized and often multifunctional compounds that are termed oxidized volatile organic compounds (OVOCs). Atmospheric OVOCs can be lost through further photooxidation (ultimately leading to CO_2 or small organic acids), condensation onto aerosol particles (forming secondary organic aerosols), or deposition to surfaces.

Due to its high emission and fast reactivity, the atmospheric oxidation of isoprene significantly impacts air quality and climate by altering the regional and global budgets of organic aerosols (2) and oxidants [e.g., ozone (3) and $HO_x = OH + HO_2$ (4)]. Fig. 1 illustrates the typical atmospheric reaction pathways for isoprene and the related monoterpenes, occurring both in the day and night. Representations of VOC oxidation and organic aerosol production in air quality and climate models have significantly improved in the last decade (3, 5) as a result of renewed focus on the isoprene chemical mechanism. This has followed from improved analytical methods that have enabled ambient and laboratory studies of the chemistry and oxidative fate of OVOCs such as isoprene hydroxy nitrates (ISOPN) and isoprene epoxydiols (IEPOX). However, little progress on understanding the dry deposition of OVOCs has been made, despite the suggested importance of this loss pathway (6, 7).

Direct and speciated measurements of trace gas exchange have been performed for inorganic compounds (e.g., O_3, SO_2, NO_x, N_2O, NH_3, HNO_3, H_2O_2), biogenic VOCs, and simple oxygenates [e.g., peroxyacetylnitrate (PAN), methanol, formic acid, acetone] (8, 9). Recent flux observations above a California orange grove provide evidence for large depositional fluxes of OVOCs (10), although the speciated fluxes were not measured. Indeed, the surface exchange behavior for the multifunctional OVOCs that comprise the majority of isoprene and monoterpene oxidation products remains poorly constrained because few ambient measurements have been performed with sufficient temporal resolution or chemical specificity. It has been postulated that dry deposition may be a significant sink for many key OVOCs within the boundary layer and thus may be a controlling factor for their atmospheric lifetimes and mixing ratios at Earth's surface. Furthermore, atmospheric model evaluations suggest that disregarding dry deposition of OVOCs may lead to a large overestimate in the formation rate of secondary organic aerosol (up to 50%) (11, 12), a larger error than that due to ignoring wet deposition (13).

Due to the scarcity of ambient chemically specific dry deposition data, model representation of atmosphere–biosphere

Significance

Dry deposition is an important removal mechanism for oxidized atmospheric compounds. This process remains, however, poorly understood due to the scarcity of direct flux observations for all but small, inorganic molecules in the atmosphere. The chemically speciated fluxes presented here comprise a unique and novel dataset that quantifies the dry deposition velocities for a variety of trace gases in a typical forested ecosystem. The data illustrate the key role of molecular diffusion in the atmosphere–biosphere exchange of water-soluble species. Furthermore, this work enabled evaluation of the dry deposition parameterization in a global chemical transport model. The results aid in resolving key discrepancies within the global model, resulting in more-accurate predictions of trace gas lifetimes and surface concentrations.

Author contributions: P.O.W. designed research; T.B.N., J.D.C., A.P.T., J.M.S.C., F.P., and G.M.W. performed research; J.D.C. contributed new reagents/analytic tools; T.B.N. analyzed data; and T.B.N. and P.O.W. wrote the paper.

The authors declare no conflict of interest.

This article is a PNAS Direct Submission.

Freely available online through the PNAS open access option.

[1]T.B.N. and J.D.C. contributed equally to this work.

[2]To whom correspondence may be addressed. Email: wennberg@caltech.edu or tbn@caltech.edu.

This article contains supporting information online at www.pnas.org/lookup/suppl/doi:10.1073/pnas.1418702112/-/DCSupplemental.

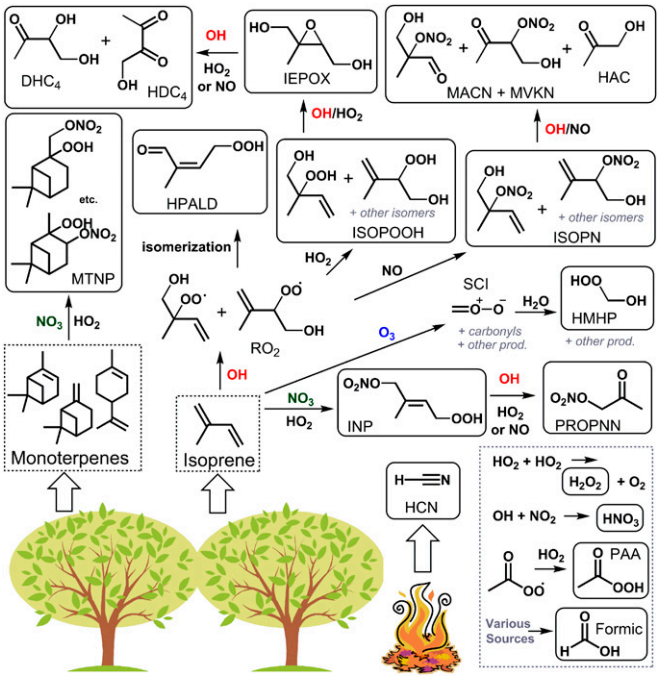

Fig. 1. Formation pathways for the oxidation products of isoprene and monoterpenes included in this study. Thick arrows indicate primary emission. Representative isomers and reaction pathways are shown. Flux data are reported for compounds shown in solid boxes. In HO_2-rich environments, the OH-initiated reaction of isoprene generates ISOPOOH, which are subsequently oxidized to epoxydiols (IEPOX) in an OH-conserving mechanism with almost quantitative yields (88). The photooxidation of IEPOX produces C_4 dihydroxy carbonyls (DHC_4), C_4 hydroxy dicarbonyls (HDC_4), HAC, formic acid, and other products (42, 89). In NO-rich environments, the minor route of the OH-initiated reaction of isoprene produces ISOPN, which are subsequently oxidized to HAC, hydroxy nitrates with backbones of MACN and MVKN, and other products (54, 90, 91). The major route of the NO-dominated OH-initiated reaction (not shown) produces carbonyls such as methacrolein, methyl vinyl ketone, and HAC, among other products. PROPNN is formed primarily from the oxidation-induced fragmentation of larger nitrates. A temperature-dependent isomerization of the isoprene RO_2 generates the HPALD (56, 92). The O_3-initated oxidation of isoprene or other exocyclic compounds forms the C_1 stabilized Criegee intermediate (SCI), among other products, which reacts with water to produce HMHP and formic acid (43). NO_3-initated oxidation of isoprene and monoterpenes, followed by the HO_2 reaction, produces INP and MTNP, respectively (93). PAA is thought to predominantly form through the HO_2 reaction with acetylperoxy radical [$CH_3C(O)OO$], which has several anthropogenic and biogenic sources (94). The main source of HCN is biomass burning (52). Formic acid has many sources, including direct emission from canopies, photooxidation at surfaces and in the gas phase, ozonolysis, and secondary chemistry (6).

exchange behavior of OVOCs rely on parameterizations that have been optimized for O_3 and SO_2 (14). The higher water solubility of oxygenates compared with hydrocarbons increases their propensity to deposit to the surface by interacting with surface water layers; thus, it is unclear if the parameterization developed for less soluble species is sufficient to describe the flux behavior of water-soluble compounds. Direct measurements of dry deposition for key VOC oxidation products are clearly needed to complete the understanding of their atmospheric fates.

As the biosphere exchange of chemical species within the boundary layer is driven by turbulence, surface fluxes can be estimated with micrometeorological methods such as eddy covariance (EC). Calculations using the EC method require mixing ratio measurements performed fast enough to capture the high-frequency timescale of turbulent eddies; e.g., measurements should exceed 1 Hz sampling frequency at this site (*SI Appendix*, Fig. S7). The recent development of fast mass spectrometry-based detectors facilitates EC flux measurements for a wide variety of species, including complex OVOCs (15). The EC flux of the desired species x (F_x) above a surface, such as a forest canopy, can be expressed as the correlation of the mixing ratio of x with the vertical wind component (w),

$$F_x = \overline{w'x'} \quad [1]$$

where primes denote deviation from the mean value, and overbars denote an average over a typical flux period (~30 min). Important underlying assumptions in Eq. **1** are that (*i*) the measurement is stationary (i.e., no significant variations in the turbulent statistics in time or in the point of measurement relative to meteorological events), (*ii*) the surface is homogeneous so that the horizontal wind components are unimportant, and (*iii*) the scale of chemical change is slow in relation to flux variation (16). In this work, we focus on the downward exchange of trace gases, where the deposition velocity (V_d, $cm \cdot s^{-1}$) is defined in relation to the flux and the mean mixing ratio of x,

$$V_d = -\frac{F_x}{\bar{x}}. \quad [2]$$

This velocity determines the deposition lifetime of compound x in the tropospheric boundary layer ($\tau_{dep} \approx h/V_d$, where h is the boundary layer height in centimeters). We report EC flux observations for 16 biogenic trace gases and energy balance closure above a southeast US temperate mixed forest in the summer. The organic and inorganic species studied here were chemically resolved with time-of-flight chemical ionization mass spectrometry using CF_3O^- reagent anions (CIMS), a soft-ionization method specific for the detection of hydroperoxides, acids, multifunctional nitrates, and multifunctional oxygenated compounds (17). The mixing ratios of compounds, meteorology, and three-dimensional wind (u, v, and w) were measured atop a 20-m walk-up tower in the Talladega National Forest in June 2013 as part of the Southern Oxidant and Aerosol Study (SOAS) campaign (*SI Appendix*, section 1).

Results and Discussion

Fluxes are calculated from the fast measurements of chemical mixing ratios (10 Hz), virtual temperature (8 Hz), and vertical winds (8 Hz). Details of the site, measurement methods, calibration (*SI Appendix*, Table S1), and quality assessment/quality control of flux data can be found in *Materials and Methods* and *SI Appendix*. The site location and tower sampling platform presented challenges to the flux measurements due to inconsistencies in fetch to the south and perturbations of wind trajectory in this direction due to shadowing by the instrument. Accurate flux measurements were possible on several days, however, when the wind direction was ideal to sample air from the forest to the north. The measurement of solar radiation, externally calibrated and converted to net radiation (18), was used as one verification of flux quality (16). The closure condition requires that the observed net radiation downward (R_n), less the storage heat flux (S) (19), is equivalent to the observed sensible heat flux upward (SH, heat that can be measured) plus latent heat flux upward (LE, heat that is used to evaporate water). The quality constraints (*SI Appendix*, section 4) were met for only a subset of measurements (~16%). We restrict our analysis to these periods.

Our observations demonstrate that dry deposition is a significant atmospheric sink for many OVOCs formed in the dark chemical and photochemical reactions of isoprene and monoterpenes. Gas-phase inorganic compounds are also observed to deposit, often quite rapidly. Fig. 2 and *SI Appendix*, Fig. S17, show downward exchanges of relevant OVOCs and inorganic species and upward exchanges of heat and water for the days in

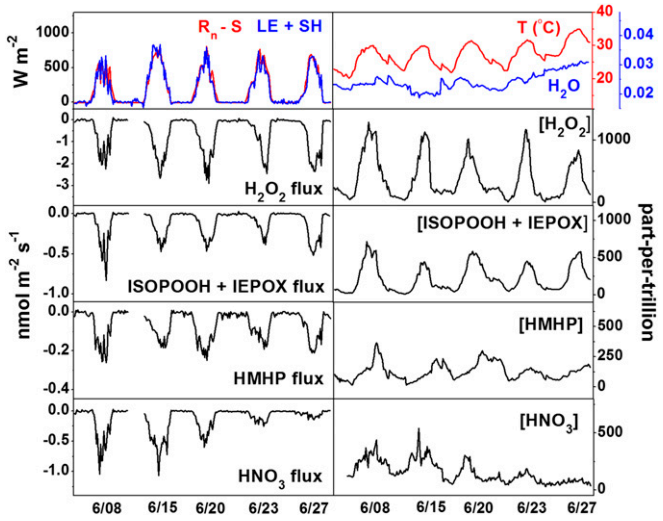

Fig. 2. The balance of latent heat (LE) and sensible heat (SH) fluxes compared with net radiation (R_n) minus heat storage (S), virtual temperature and absolute water vapor, and fluxes and mean mixing ratios for select chemical species. *SI Appendix*, Fig. S17, shows the remaining fluxes and mean mixing ratios measured in this work.

this study. LE comprised the majority of the total upward energy flux at this site, which is typical for forested environments. Fluxes of hydrogen peroxide (H_2O_2) are among the largest observed during the campaign, reaching 2 nmol·m^{-2}·s^{-1}, in good agreement with other accounts in forested settings (20). Observed fluxes had a daytime diurnal pattern, driven by the combined effect of light and temperature on turbulence, stomatal conductance, and gas-phase photochemical production.

The biosphere–atmosphere exchange behaviors for several species studied here are currently unknown or have only been speculated in the past. These chemical compounds include hydrogen cyanide (HCN), hydroxymethyl hydroperoxide (HMHP), peroxyacetic acid (PAA), the sum of isoprene hydroxy hydroperoxides and epoxydiols (ISOPOOH + IEPOX), isoprene hydroperoxy aldehydes (HPALD), ISOPN, the sum of hydroxy nitrates with carbon backbones of methacrolein and methyl-vinylketone (MACN + MVKN), propanone nitrate or propanal nitrate (PROPNN), hydroxyacetone (HAC), the C_4 hydroxy dicarbonyl from IEPOX oxidation (HDC_4), the C_4 dihydroxy carbonyl from IEPOX oxidation (DHC_4), isoprene nitrooxy hydroperoxide (INP), and monoterpene nitrooxy hydroperoxide (MTNP). The structures of the compounds measured in this work are shown in Fig. 1.

Fig. 3 shows the observed mean deposition velocities (V_d) for each compound binned into hourly periods. Daytime V_d values (Fig. 3 legend) were averaged for local hours 1000–1500 across all measurement days. In most cases, the deposition velocities are more rapid than that of O_3 (21). Diurnal patterns of deposition velocities largely mirrored those for flux. However, the diurnal patterns for some compounds are asymmetric (peaking before noon), which may indicate that their biosphere exchange is controlled in part by stomatal conductance and/or surface water availability. Although daytime V_d may depend to some extent on environmental conditions and canopy characteristics at each site, it is instructive to compare the values measured here with available data on dry deposition over forests. For example, in this work, the observed V_d for H_2O_2 (5.2 ± 1.1 cm·s^{-1}) is in excellent agreement with other direct measurement accounts (V_{d,H_2O_2} = 5 ± 2 cm·s^{-1} (22–24). Measured fluxes of formic acid have been reported to be bidirectional, with an effective range of $V_{d,Formic}$ = 0.17–1.0 cm·s^{-1} (25, 26) that is in reasonable agreement with our determination (1.0 ± 0.4 cm·s^{-1}). Measurements of nitric acid (HNO_3) dry deposition encompass the largest range in the literature [V_{d,HNO_3} = −1–8 cm·s^{-1} (27–30)]. HNO_3 is a challenging compound to measure because of its interactions with instrument surfaces. The CIMS measurement of HNO_3 was affected by an instrumental delay and was corrected with a time response perturbation function (*SI Appendix*, section 5). Our determination for nitric acid deposition velocity (V_{d,HNO_3} = 3.8 ± 1.3 cm·s^{-1}) is within range of other reports and is consistent with results from resistance modeling performed in this work. Other speciated V_d we observe compare well, although indirectly, to previously reported data available as averaged measurements within the class of organic hydroperoxides [$V_{d,ROOH}$ = 1.1–2.5 cm·s^{-1} (22, 23)] or organic nitrates [$V_{d,RONO_2}$ (gas + particles) ≈ 2.0 cm·s^{-1} (29, 30)].

Resistance Model of Deposition. Here we seek to evaluate the physical factors that control dry deposition within the framework of resistance modeling. Deposition velocity is usually parameterized as a series of resistances in the transport from the atmosphere to a surface—in this case, a canopy that is represented as a theoretical large leaf (31). The downward trajectory of a chemical species can be hindered by the step-wise resistances to aerodynamic transfer (R_a), molecular diffusion through the quasi-laminar boundary layer of the leaf (R_b), and uptake at the surface of the leaf (R_c),

$$V_d = \frac{1}{R_a + R_b + R_c} \quad [3]$$

SI Appendix, section 6, describes the resistance model in detail. We used R_a and R_b parameterization as suggested (32–34). R_a is dependent only on the atmospheric stability (i.e., turbulence). R_b is inversely dependent on the turbulence, the molecular diffusivity of compound x in air [D_x (m^2·s^{-1})], and canopy characteristics such as the observed leaf area index (LAI) of the canopy at the measurement site (LAI = 4.7; see *SI Appendix*). R_c is parameterized according to a revised Weseley scheme (35), which, to first order, considers the combined resistances from stomata (r_s), mesophyll (r_m), and cuticles (r_{cu}) of plants. The surface uptake of

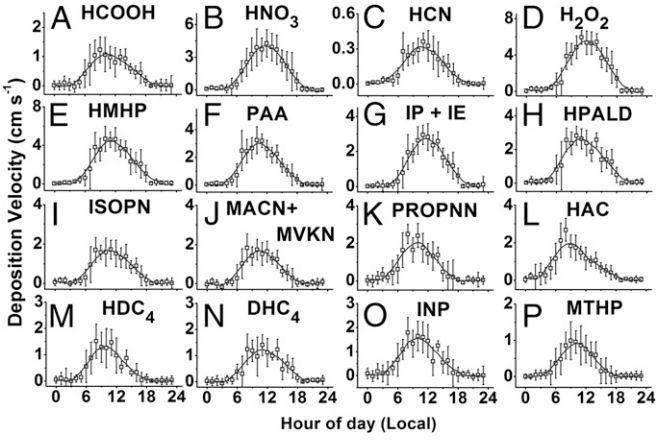

Fig. 3. Measured deposition velocities (centimeters per second) for species included in this work. The daytime (h = 1000–1500) mean (centimeters per second) and SD (1σ) are (*A*) formic acid [1.0 ± 0.4], (*B*) nitric acid [3.8 ± 1.3], (*C*) HCN [0.3 ± 0.1], (*D*) H_2O_2 [5.2 ± 1.1], (*E*) HMHP [4.1 ± 1.1], (*F*) PAA [2.7 ± 0.7], (*G*) ISOPOOH + IEPOX (IP + IE, isomeric) [2.5 ± 0.6], (*H*) HPALD [2.4 ± 0.6], (*I*) ISOPN [1.5 ± 0.6], (*J*) MACN + MVKN [1.5 ± 0.5], (*K*), PROPNN [1.7 ± 0.6], (*L*) HAC [1.4 ± 0.5], (*M*) HDC_4 [1.1 ± 0.5], (*N*) DHC_4 [1.0 ± 0.4], (*O*) INP [1.3 ± 0.6], and (*P*) MTNP [0.8 ± 0.4]. Solid curve is data smoothed by a moving average algorithm.

a particular compound is represented as functions of D_x, water solubility (H, Henry's Law coefficient), and a reactivity coefficient (f_0, range 0–1 where 1 is as reactive as ozone),

$$R_c \sim \left(\frac{1}{(r_s(D_x) + r_m(H, f_0))} + \frac{1}{r_{cut}(H, f_0)} \right)^{-1}. \quad [4]$$

The original Weseley parameterization overestimates R_c for compounds like H_2O_2 (20), which should be close to zero (22), despite the fact that water solubility of H_2O_2 is not significantly variable below pH = 8 and f_0 is set to maximum. With empirical results at hand, we optimized the parameters in the Weseley R_c scheme to minimize discrepancies between calculated and observed V_d. We adjusted coefficients only in the r_m and r_{cut} terms (*SI Appendix*, Eqs. **14–16**) to be more sensitive to water solubility. Furthermore, we use the simple Henry's Law coefficients (H) that describe physical solvation in pure water, instead of effective Henry's Law coefficients (H^*). We find that H satisfactorily reproduces empirical R_c. Furthermore, H is a more practical parameter as the knowledge of ionic activity (36, 37) and pH at surface aqueous layers is not readily available to estimate H^* for the species where solubility enhancements are important (e.g., aldehydes, acids, and bases). We neglect pH dependence for solubility because pH inside plant mesophyll (38) and leaf surface (39) tend to be buffered near neutral. H was estimated based on chemical proxies for the larger multifunctional compounds (*SI Appendix*, Table S2) where measured values were unavailable (40).

Fig. 4 shows that results from the revised resistance model are in excellent agreement with ambient observations for the majority of the compounds studied in this work. The poorer model agreement for the mean of ISOPOOH + IEPOX is likely due to error in flux measurement and not modeling. Deposition velocity for IEPOX may be slightly underrepresented in our work because the expected time response delay in sampling IEPOX was uncorrected (*SI Appendix*, section 5). Surface resistances are small for the water-soluble and more reactive species (e.g., strong acids, hydroperoxides, and peroxyacids) but become important for other compounds. The parameterization captures observed V_d successfully on both ends of the water-solubility spectrum, e.g., for poorly water-soluble compounds like HCN [$H \approx 10$ M·atm^{-1} (40)] and for highly water-soluble compounds like HMHP ($H \sim 10^6$ M·atm^{-1}).

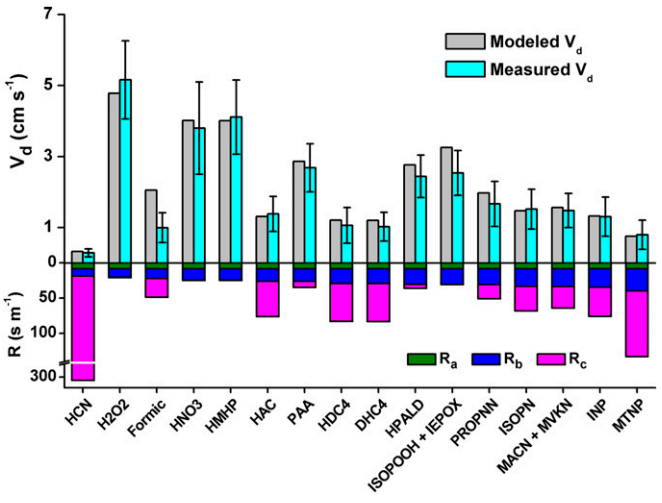

Fig. 4. (*Upper*) Daytime mean deposition velocities (centimeters per second) that were measured vs. calculated by a tuned resistance model. (*Lower*) Modeled contributions to the total deposition resistance from aerodynamic transfer (R_a), molecular diffusion (R_b), and canopy uptake (R_c). Model inputs and results are shown in *SI Appendix*, Table S2.

The exception is formic acid, where V_d predicted by the resistance model is approximately twice the observed value.

The behavior of formic acid cannot be explained by the physical characteristics of this molecule. With the assumption that the resistance model results are robust, poor model agreement implies that error may exist in the formic acid measurement, solubility estimations, or the assumption that formic acid has no emission source. A time response test suggests that >98% of the formic acid flux was captured by the measurement (*SI Appendix*, Fig. S11) and H is not expected to be overestimated for formic acid. More likely, we believe that a significant portion of the observed formic acid in a forested setting is produced by secondary, possibly heterogeneous, reactions (6, 41). These secondary emission pathways are additional to the proposed primary emission of formic acid from biogenic, anthropogenic, and pyrogenic sources. The discrepancy between modeled and observed V_d of formic acid requires a large emission flux—on the order of 1 nmol·m^{-2}·s^{-1} in the daytime.

One possible route to secondary formic acid formation may include water-mediated degradation of larger OVOCs that are deposited on canopy surfaces or on aerosol surfaces, e.g., the oxidation of IEPOX (42) and decomposition of HMHP (43). The deposition of HMHP and IEPOX is likely independent of surface chemistry at this site because surface uptake is not a limiting process for these compounds (Fig. 4, *Lower*). Thus, their in-canopy chemistry is not expected to lead to model/measurement disagreement, within the error of the measurement, by significantly enhancing deposition. HMHP decomposition (downward flux of ~0.2 nmol·m^{-2}·s^{-1}) may produce formic acid via thermal, photochemical, or dark decomposition pathways. The lifetime of HMHP with respect to hydrolysis at neutral pH has been measured to be roughly 17 min (44), on the timescale of mixing within the canopy. The formation yield of formic acid from IEPOX oxidation is significant in the gas phase (10–30%) (42), although the lifetime of IEPOX in the gas phase is long (>10 h). We speculate the yields are higher in the aqueous phase; however, more work is needed before the contribution of IEPOX to the formic acid flux can be estimated.

Another possible formic acid source is the rapid in-canopy ozonolysis of monoterpenes and other biogenic VOCs (45, 46), which may occur primarily within stomata (47) and is enhanced under humid conditions (43). For example, the in-canopy ozonolysis of sesquiterpenes ($\tau \approx$ 1–2 min) has been estimated to consume 0.6–1.5 nmol·m^{-2}·s^{-1} (7–28%) of the downward ozone flux and 46–61% of the sesquiterpenes mass in Amazonia (48). Approximately 6% of the ozone flux at this site is required to account for the entire formic acid flux. Although the kinetics and yields of the myriad formic acid formation routes are not well understood, a 1 nmol·m^{-2}·s^{-1} secondary source of formic acid from these combined pathways appears plausible.

The calculated resistances shed light on a remarkable empirical relationship of highly depositing compounds—their observed daytime deposition scale with inverse molecular mass $(\sqrt{m})^{-1}$ (Fig. 5). These trends suggest that molecular diffusivity through the leaf boundary layer and, for larger molecules, from the leaf surface itself act as a constraint on dry deposition at a specific turbulent condition. According to the resistance model, diffusivity restrictions arise from the terms describing transport to the quasi-laminar layer of the leaf surface (R_b) or through stomata (r_s component of R_c). We find two "diffusion-limited" upper bounds: when there is no resistance at the surface of the leaf ($R_{total} = R_a + R_b$, Fig. 5, dashed line) and when there is a stomata-controlled resistance at the surface of the leaf [$R_{total} = R_a + R_b + R_c$ (r_s), Fig. 5, solid line]. The two limits converge for smaller compounds (<80 Da) with high diffusivity such that r_s is minimal. As expected, the observed daytime V_d for HNO_3 (the prototypical molecule for rapid deposition) is at maximum for its size. It appears that bulkier compounds such as MTNP cannot achieve surface resistance-free deposition because they are hindered by subsequent transport through the stomata.

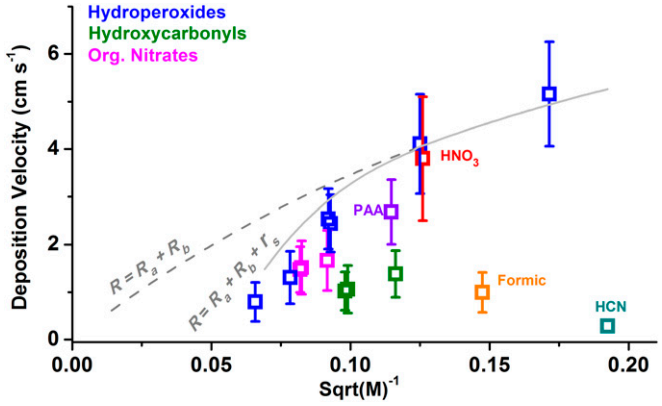

Fig. 5. The dependence of deposition velocities on inverse molecular mass $(\sqrt{m})^{-1}$, a representation of molecular diffusivity, for various chemical classes. The dashed line is the upper limit for deposition without surface resistance ($V_d = 1/[R_a + R_b]$). The solid line is the upper limit for deposition that experiences only stomatal resistance at the surface ($V_d = 1/[R_a + R_b + R_c\,(r_s)]$).

Efficiently-depositing compounds approaching the stomata-controlled diffusion limit generally belong to the chemical classes of simple or multifunctional hydroperoxides and strong acids with high water solubility (threshold H in this model $\approx 3 \times 10^4$ M·atm^{-1}). The model sensitivity to various parameters is discussed in *SI Appendix*, section 6, and shown in *SI Appendix*, Fig. S16, for H. Organic nitrates and peroxyacids are close to the upper bound. Most of the major outliers in Fig. 5, e.g., HCN and ketones, have poor solubility in water or low reactivity at the leaf surface, which produces a substantial nonstomatal R_c term. In particular, uptake of HCN from the surface comprise >90% of its total resistance. Formic acid is also an outlier on this plot, likely due to the aforementioned emission. In addition to diffusion restrictions, the absolute deposition velocities for a specific compound remain highly dependent on atmospheric stability. The aerodynamic resistance (R_a) can be significant when the atmospheric stability is high; however, this term is identical for all compounds, so it will materialize as a vertical offset in Fig. 5. Under exceptionally high turbulent mixing conditions ($R_a \rightarrow 0$), we estimate that V_d for HNO_3 and H_2O_2 can reach ~6 cm·s^{-1} and 8 cm·s^{-1}, respectively, in this forest setting.

The empirical relationship between mass and deposition velocity for soluble species serves as a useful paradigm for understanding previous and future measurements performed under differing conditions. That a single physical characteristic of atmospheric trace gases constrains their deposition velocities in relation to each other has not yet been fully realized. Current sensitivity simulations of atmospheric loss often exceed these "diffusion-limited maxima" when modeling dry deposition of OVOCs. For example, HNO_3 is typically modeled to have the highest relative deposition velocity, and sensitivity studies tend to equate V_d of other compounds that may also deposit quickly (e.g., ISOPN) to V_d of HNO_3 (7, 49). These data suggest that it may be more appropriate to scale V_d of highly depositing species in sensitivity simulations with respect to H_2O_2 or HNO_3 based on molecular mass. Furthermore, it appears that H_2O_2 will always deposit faster than HNO_3 at any given turbulent condition.

Impact on Regional and Global Budgets of Trace Gases. Global atmospheric transport models used to assess chemistry and climate feedbacks often overpredict surface volume mixing ratios for trace gases such as H_2O_2 (50, 51), HCN (52), and ISOPN (5). Depending on the molecule, such model discrepancies can affect the entire troposphere or only the boundary layer. These overestimations have motivated hypotheses about unknown atmospheric sinks for these compounds or their precursors, e.g., enhanced aerosol uptake of HO_2 due to Fenton chemistry that does not produce H_2O_2 in the gas phase (51) or an ocean sink for HCN (52).

We performed regional and global simulations using GEOS–Chem v9.2 (53), a global 3D chemical transport model, to assess the importance of dry deposition in model simulations of surface mixing ratios. GEOS–Chem simulations were driven by GEOS-FP (forward processing) meteorology with hourly resolution (*SI Appendix*, section 7). Compound-specific surface mixing ratio and vertical profile impacts in response to modeled changes in dry deposition are a nonlinear result of chemistry, land use, and meteorology; thus, they are not possible to predict a priori. In one case study, we performed a 1-mo simulation at a fine-grid horizontal resolution of 0.25° × 0.33° to facilitate comparisons with hourly observations of deposition velocities and meteorology at the measurement site. Two year-long global simulations at a coarser resolution (2° × 2.5°) were also performed for a "base" case and "sensitivity" case. In the base simulation, we use the default GEOS–Chem dry deposition velocities, while in the sensitivity simulation, we adjust the average daytime V_d of several compounds to match measurements. We use the most recent version of GEOS–Chem chemical mechanism with a few updates (*SI Appendix*, Table S3) to reflect revised knowledge of OVOC reactions published very recently, such as updated ISOPN + OH and ISOPN + O_3 rate coefficients (54). Model results for HCN and several other species of interest are not available because these compounds are either not included in GEOS–Chem (HMHP, HCN, HPALDs, HDC_4, DHC_4, INP, and MTNP) or because their dry deposition was neglected in the model (PAA). Among the compounds not included in the simulations, HMHP (55) and HPALDs (56) may have the more significant impact on model predictions because of their high deposition velocities and large abundance in forested settings and in biomass burning plumes.

Fig. 6 shows the meteorological conditions and energy fluxes generated by GEOS-FP and deposition velocities calculated by the fine-grid GEOS–Chem simulation for June 2013 at the coordinates of measurement site (CTR). Excellent agreement in both the mean magnitudes and diurnal pattern was obtained for the comparison of friction velocity (turbulence, Fig. 6*A*), sensible heat flux (Fig. 6*B*), and latent heat flux (Fig. 6*C*) between the model (averaged for 30 d) and measurements (averaged for 5 d). This suggests that the meteorological and surface exchange conditions during the select days used in this work are representative of the site during June. Furthermore, these simulations suggest that flux observations during the SOAS campaign are not atypical for the eastern US region or for the year 2013 (*SI Appendix*, Figs. S18 and S19, respectively).

The deposition velocities for compounds of interest showed poorer agreement in the fine-grid simulations (Fig. 6 *D–F*, black lines). As meteorology and land surface processes are reasonably well represented in the atmospheric model, the discrepancy likely resides in the parameterization of surface uptake resistance (R_c) by the canopy. The GEOS–Chem model uses the Weseley scheme (Eq. **4**) to calculate surface resistance for chemical species. As noted earlier (20), R_c for H_2O_2 and certain OVOCs are overestimated compared with observations, leading to low values of V_d simulated by the model. For the sensitivity study, we arbitrarily increased the effective solubility inputs for compounds of interest (*SI Appendix*, Table S4) until the calculated V_d matched observed values (Fig. 6 *D–F*, blue lines, when an applicable change is made). In some cases, the required solubility adjustments are clearly too large compared with uncertainties and suggest that a change to the parameterization, such as was done in *Resistance Model of Deposition*, should be implemented to improve the model description of dry deposition in future work. This method, however, is a reasonable temporary solution that can be

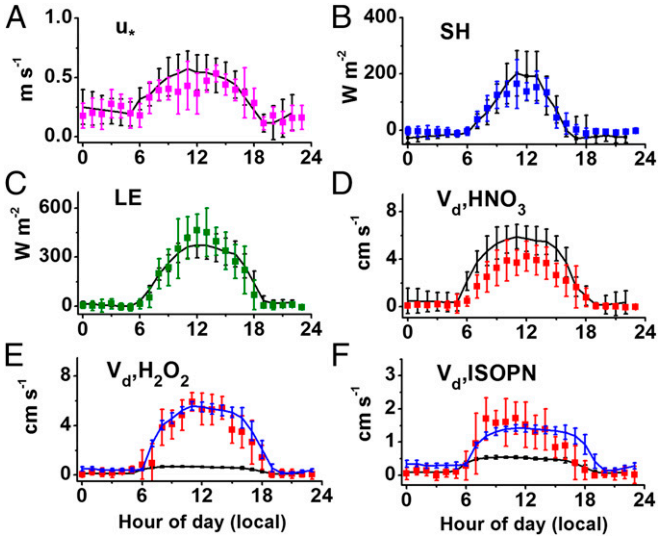

Fig. 6. Base GEOS–Chem (run at 0.25° lat × 0.33° lon) simulations (black lines) and observations (colored points) for June 2013 at the Brent, AL CTR site. The modeled (*A*) friction velocity, (*B*) sensible heat flux, and (*C*) latent heat flux data are derived from GEOS-FP hourly-resolved meteorology. Deposition velocities (*D–F*) were calculated from GEOS–Chem without modifications (black lines) or with adjustments to the Henry's coefficient of these compounds (blue lines, if applicable) for a sensitivity study (see text). Simulations were performed for all 30 d in June 2013, and observed data were measured for the 5 d included in this study. Error bars represent 1 SD from mean values.

immediately implemented in atmospheric models while an updated parameterization is under development.

Table 1 shows simulation results extracted for June 2013 from the base and sensitivity studies in the grid box that encompasses the coordinates of the measurement site. Changes in V_d significantly impact predictions of surface concentration for the depositing species, but secondary chemistry, e.g., ozone production or SO_2 oxidation, are not considerably affected. The surface mixing ratios for compounds with adjusted V_d decreased ~10–50%. Although the observed changes in modeled mixing ratios were not found to affect O_3 and HO_x ($OH + HO_2$) at this site, season, and altitude (<1 km), effects on O_3 and HO_x due to the photochemistry of isoprene nitrates and H_2O_2, respectively, may be more significant for other regions of the globe and times of the year (51, 57). The adjustment in V_d for H_2O_2 was the largest (a factor of 7 increase), and its surface mixing ratio was correspondingly reduced by the greatest amount (45%). Higher H_2O_2 dry deposition significantly affected simulation results of its surface concentration for much of the forested areas of the globe (Fig. 7), e.g., Canadian and European boreal forests, the Amazon basin, and the Congo basin. Measurements at these sites are not available for model comparison; however, the results suggest that underrepresentation of dry deposition for H_2O_2 is likely responsible for much of past overestimations of its mixing ratios in GEOS–Chem simulations (51).

The sensitivity of H_2O_2 boundary layer mixing ratio to dry deposition may be expected because this compound has a long lifetime with respect to oxidation and photolysis in the lower atmosphere. To estimate dry, midday sinks, we use measured daytime deposition velocities (Fig. 3), simulated [OH] ≈ 2.6×10^6·cm^{-3} (twice the 24-h value in Table 1), simulated photolysis under tropical noon with 300 Dobson units ozone (58), and a boundary layer height of 1.5 km. The deposition lifetime of H_2O_2 ($\tau_{dep} \approx 8$ h) accounts for >70% of its total atmospheric loss under dry conditions [$\tau_{hv} \approx 1.4$ d; $\tau_{OH} \approx 2.6$ d (59)]. Reaction with ozone, usually several orders of magnitude slower for unsaturated compounds and unimportant for saturated compounds, was neglected as a loss process. Dry deposition of other saturated compounds can be expected to dominate their atmospheric removal in a manner similar to H_2O_2 because their reactive lifetimes in the atmosphere are long and their water solubilities are high. For example, HMHP (~4 cm·s^{-1}) has a deposition lifetime of 10 h, accounting for ~55% of its atmospheric removal [$\tau_{hv} \approx 4$ d, $\tau_{OH} \approx 14$ h (estimated based on methylhydroperoxide+OH rate coefficient) (60)]. Similarly, dry deposition may comprise ~60% of the atmospheric loss for PAA (59, 61) and ~45% of the atmospheric loss for IEPOX (42). IEPOX is also removed by reactive uptake to aerosols. Using data from a recent

Table 1. GEOS–Chem base and sensitivity (sens.) simulation for the grid box representing the Brent, AL, field site, 2° × 2.5° resolution

Tracer name	Base V_d,* cm·s^{-1}	Sens. V_d,* cm·s^{-1}	Base conc. (70 m)	Sens. conc. (70 m)	Δ %
OH	–	–	1.32×10^6	1.30×10^6	−2
HO_2	–	–	3.84×10^8	3.77×10^8	−2
NO	–	–	0.12	0.12	0
NO_2	–	–	0.98	0.98	0
O_3	–	–	50.97	50.63	−1
PAN	–	–	0.38	0.37	−2
HNO_3	3.02	3.02	0.46	0.45	−1
H_2O_2	0.37	2.66	2.83	1.55	−45
PPN	–	–	0.019	0.018	−2
HCHO	–	–	3.64	3.60	−1
MHP	–	–	1.18	1.15	−2
SO_2	–	–	1.20	1.21	1
SO_4	–	–	0.53	0.52	−2
ISOPN	0.30	0.82	0.081	0.073	−10
MACN+MVKN	0.30	0.81	0.075	0.069	−9
PROPNN	0.30	0.48	0.055	0.047	−14
HAC	0.30	0.71	1.48	1.25	−15
ISOPOOH	0.76	0.76	0.38	0.38	0
IEPOX	2.86	2.73	0.58	0.59	1

Concentrations (conc.) are reported in parts per billion by volume, except OH and HO_2, where units are in molecules per cubic centimeter. Percent change is defined with respect to the base simulation.
*The 24-h average (approximately half of daytime value).

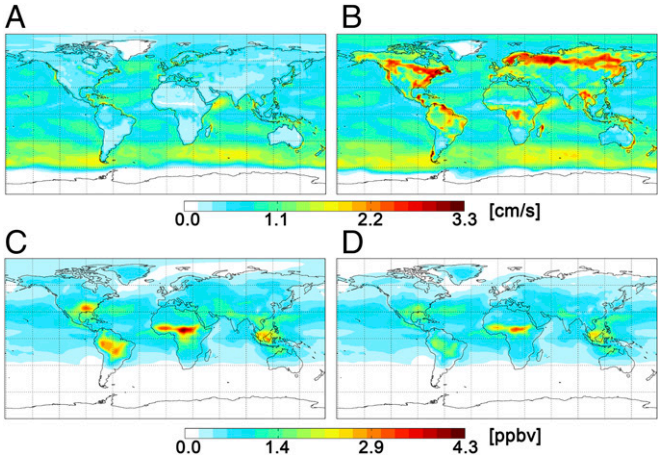

Fig. 7. GEOS–Chem sensitivity study (2° lat × 2.5° lon) for H_2O_2 during June 2013: 24-h mean deposition velocities in the (*A*) base and (*B*) sensitivity simulations and surface mixing ratios in the (*C*) base and (*D*) sensitivity simulations.

laboratory study of IEPOX particle uptake probabilities (62), we estimate that the dry deposition fate of IEPOX is significantly affected only in the presence of very acidic inorganic sulfate particles at pH < 1 (reduced to ~20%) and is relatively unaffected if the particles have more moderate acidities (pH > 3).

For unsaturated compounds like ISOPN, deposition may comprise a smaller fraction (<10%) of the daytime sink because its reaction with OH is fast (54). Thus, errors in representation of ISOPN dry deposition will have a much smaller effect on simulated ISOPN surface concentrations. In general, while dry deposition is less important for organic nitrates than peroxides, changes in their mixing ratios obtained from the sensitivity study were significant for both classes of compounds. Mixing ratios for organic nitrates from isoprene were reduced by 9–14% in the sensitivity study. The carbonyl nitrates (in particular MACN) may be reasonably photolabile (63), further diminishing the importance of dry deposition. Smaller multifunctional carbonyls like HAC are longer-lived in the atmosphere. Correspondingly, their surface concentration reductions (15%) in the sensitivity study are larger than for ISOPN.

The differences in H_2O_2 and other trace gas mixing ratios in the troposphere between the base and sensitivity studies were most significant within the boundary layer (<3 km). Importantly, the concentration gradient is larger near the surface when V_d is higher (*SI Appendix*, Fig. S20), leading to more pronounced differences between the base and sensitivity studies at the measurement height of ~20 m. As the lowest vertical layer in GEOS–Chem corresponds to an average height of 70 m, we linearly extrapolated the surface gradient to the tower height for compounds of interest to compare with measurements. Compared with mixing ratios measured at SOAS [24-h mean ≈ 0.5 (±30%) parts per billion by volume (ppbv) on campaign days without significant precipitation], H_2O_2 mixing ratios are overpredicted by more than 300% in the base simulation and are much closer in the sensitivity simulations, but still overpredicted by ~85%. Daytime values for other trace gases are still overestimated by 30–300% in the model for the CTR measurement site; however, all mixing ratios in the sensitivity study are substantially closer to measured values at SOAS when extrapolated to the measurement height. The errors in overestimations are reduced by factors of 1.5–4.

The most dramatic overestimation occurred with IEPOX, where 24-h mean values at SOAS are measured to be ~0.09 ppb with tandem mass spectrometry and simulated to be ~0.35 ppb (extrapolated to 20 m). Unlike H_2O_2, this result is not attributed to underestimation of dry deposition. In fact, the simulated V_d in GEOS–Chem for IEPOX is ~70% higher than results from the adjusted resistance model we used in this work. Interestingly, V_d simulated in GEOS–Chem for ISOPOOH is ~50% lower than our estimates. IEPOX deposition velocity should be limited by molecular diffusion due to its high water solubility (Fig. 5), which suggests a lower daytime V_d than that simulated by GEOS–Chem (~5.5 cm·s^{-1}). The average V_d for these isobaric species was not adjusted in our sensitivity simulations because their mean simulated V_d is similar to the observed value due to the negating errors. More likely, the low observed mixing ratios of IEPOX at SOAS may be due to error in its production rate or because heterogeneous loss reactions, such as conversion to organic aerosols in anthropogenically impacted particle liquid water (64), were not accounted for in the model. IEPOX uptake clearly involves hydronium-catalyzed ring opening in aerosol liquid water (62, 65, 66). However, field results suggest that more factors than acid catalysis govern the chemistry (67). Laboratory results indicate that hydrated ammonium sulfate particles (but not sodium or magnesium sulfate) produce a similar magnitude of organic aerosol mass due to IEPOX uptake regardless of whether acid was added (68, 69). More work is needed to elucidate field observations and update atmospheric model mechanisms.

Results from this sensitivity simulation suggest that improved representations of dry deposition in GEOS–Chem, and likely other models, would partially resolve model overestimations for certain species within the boundary layer. Additionally, an experimentally constrained OVOC dry deposition scheme is likely to have a substantial effect on the organic aerosol budget, as suggested previously (11). The impact on aerosols, however, was not determined in this work. Enhanced accuracy of model simulations of biogenic trace gas surface concentrations and lifetimes may be gained by updating the model to include OVOCs that are not yet in the mechanism and by improving vertical mixing schemes for volatile compounds (70), especially near the canopy (71).

Impact on Ecosystems. The field observations suggest that a significant portion of VOC emitted by the biosphere is returned to the ecosystem via dry deposition of OVOCs. Fig. 8, *Left*, shows the net mean deposition of C, N, and O atomic mass, obtained from the speciated contributions of 16 molecular formulas observed, averaged across multiple days. As our measurements encompass only a subset of organic species present in the troposphere, all estimations of combined fluxes are lower limits. We observed that at least 6% of the reactive carbon mass that was emitted as isoprene in an AL forest [~4 mgC·m^{-2}·h^{-1} daytime (72), integrated over 24 h] were removed by the canopy via dry deposition of isoprene's oxidation products. Our analysis does

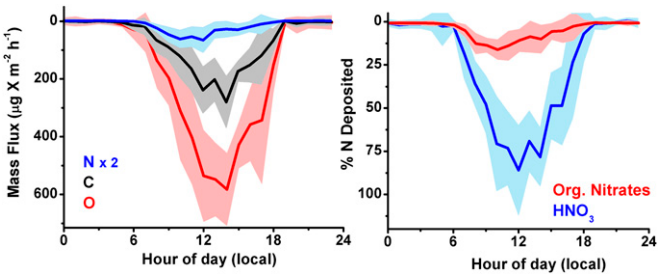

Fig. 8. (*Left*) Net carbon, oxygen, and nitrogen downward flux by mass, calculated from molecular formulas for compounds shown in *SI Appendix*, Table S1, and averaged over the dates in the study. (*Right*) Percent contribution of organic nitrates and nitric acid to the measured oxidized nitrogen flux.

not include HCN and MTNP. This estimate of the contribution of dry deposition removal of isoprene carbon may be larger if the many isoprene-derived OVOCs that are expected to deposit are included in the analysis, e.g., ethanal nitrate, various acylperoxynitrates (APNs), acetic acid, glycolaldehyde, formaldehyde, glyoxal, methylglyoxal, acetaldehyde, and other OVOCs.

Oxygenated compounds contribute most of the mass flux due to the combined effect of their larger molecular weight from the incorporation of oxygen during oxidation (73), and the propensity for less-volatile and more-water-soluble compounds to deposit. The oxidant deposition observed by our instrument is attributed to hydroperoxides (–OOH), although we are missing the likely minor contribution of methyl hydroperoxide (MHP). Organic hydroperoxides can be formed primarily from the RO_2 reaction with HO_2, more prevalent in pristine environments, or from humid ozonolysis, more prevalent in urban-influenced environments (Fig. 1). Thus, oxidant deposition is highly dependent on geographical location and time of day. However, ozone has been considered as the predominant oxidant in modeling dry deposition or in estimating oxidant-induced plant damage. The apparent effects of ozone on forest ecosystems are well documented, but they may not be directly attributable to ozone. Ozone concentration rapidly declines after stomatal uptake, and damaging effects in plants are often linked to the production of secondary stressors that are dependent on ozone dose (74). These secondary stressors were suggested to be, in part, H_2O_2, HMHP, and other hydroperoxides that are produced as part of alkene ozonolysis (46). It should be noted that both H_2O_2 and O_3 may elicit beneficial defense reactions in plants below their relative phytotoxic limits (75, 76), and the physiological effects are tightly coupled. Thus, it may be useful to consider the total activated oxygen flux as the sum of ozone and peroxides.

We estimate that the daytime molar peroxide flux at this southeast US site (2.4 nmol $OOH \cdot m^{-2} \cdot s^{-1}$) is 15% of the ozone flux on average [~16 $nmol \cdot m^{-2} \cdot s^{-1}$ using $[O_3]$ = 50 ppbv and $V_{d,O_3} = 0.8\ cm \cdot s^{-1}$ (77)]. However, in more pristine areas like the Amazon rainforest, the concentration of total peroxides is higher and ozone is lower than the southeast United States. The estimated daytime peroxide flux of 5.7 $nmol \cdot m^{-2} \cdot s^{-1}$ in Amazonia [using $[H_2O_2]$ and [ROOH] observed by Lelieveld et al. (4) and $V_{d,H_2O_2} = 5\ cm \cdot s^{-1}$ and $V_{d,ROOH} = 2\ cm \cdot s^{-1}$] can be 50–120% of observed daytime O_3 fluxes during the dry season (78). These results suggest that, across varying degrees of urban influence, peroxides can comprise a significant to dominant fraction of the daytime oxidant flux in forest ecosystems.

Exogenous H_2O_2 (millimolar equivalent) has been shown to inhibit stomatal opening by signaling the production of NO in guard cells (79, 80). Furthermore, as peroxides are potent oxidizers and generators of reactive oxygen species (ROS) like the hydroxyl radical (OH) and the superoxide ($O_2^{\cdot -}$) in water, their large deposition flux motivates inquiries into their fates at the surface of plants. Deposited peroxides likely participate in aqueous or heterogeneous chemistry, e.g., the oxidation of deposited SO_2 to sulfuric acid (81) or the production of ROS like OH, HO_2, and $O_2^{\cdot -}$ through direct photochemistry and catalytic reaction with trace metals (Fe) (82). During the SOAS campaign, we measured plumes of SO_2 in the range of 1–9 ppb (*SI Appendix*, Fig. S21). The peroxide-mediated production of strong acids and oxidants may play a role in plant damage during these episodes. Additionally, this chemistry may contribute to the aforementioned inferred emission flux of formic acid through heterogeneous oxidation of OVOCs. Whether the observed deposition flux of peroxides can impact atmospheric chemistry via heterogeneous pathways or affect plant function under typical atmospheric conditions remains to be further explored.

The mean daytime dry deposition flux from HNO_3, HCN, and speciated organic nitrates was measured to be 27 (±15) $\mu gN \cdot m^{-2} \cdot h^{-1}$. To estimate the ecosystem input of nitrogen, the dry flux of N-containing species that were not measured in this work (NH_3, NH_4^+, etc.) were simulated with GEOS–Chem. The wet-deposited N data for 2013 (measured as NH_4^+ and NO_3^-) was provided by the National Atmospheric Deposition Program at the AL03 site corresponding to CTR (nadp.sws.uiuc.edu/). We estimate that dry deposition supplied ~52% of the total wet and dry input of nitrogen to the canopy by mass. This result is consistent with average estimates (~46%) at 10 North American forests (83).

HNO_3 is commonly assumed to dominate the oxidized nitrogen dry deposition flux; however, our data indicate that organic nitrates ($RONO_2$) measured by our instrument can constitute a sizable portion (15%) of the dry flux of oxidized nitrogen observed at this site (Fig. 8, *Right*), with nitric acid making up the balance. This is a lower limit of the organic nitrogen input into the canopy. Zhang et al. (49) assumed a deposition velocity of isoprene nitrates to be ~5.5 $cm \cdot s^{-1}$ in the daytime (greater than a factor of 3 larger than our observations) and arrived at a similar conclusion. If we include an estimation for acylperoxy nitrates from data obtained in Northern California (84), the resulting organic nitrogen contribution would be a bit higher (~25%). HCN was, at most, 3% of the N flux observed in this work. However, the main source of HCN is biomass burning and, thus, its flux will vary significantly depending on location and time of year. The minor impact from NO_2 deposition (21) was neglected. The data demonstrate that organic nitrogen is an important fraction of the oxidized nitrogen dry deposition flux, similar to wet deposition (85). The organic nitrogen may be taken up by foliage (86, 87) and incorporated into the synthesis of leaf nutrients. As the effects of organic nitrogen on carbon sequestration are inadequately represented in most ecological models, these data motivate further inquiry into the ecosystem ramifications of OVOC deposition.

Materials and Methods

Site and Sampling. This work was performed as part of the SOAS Campaign (soas2013.rutgers.edu/) at the CTR Southeastern Aerosol Research and Characterization Study (SEARCH) site operated by the Electric Power Research Institute (Brent, AL, Lat 32.90289 Lon –87.24968) for the US Environmental Protection Agency. The metal walk-up sampling tower was ~20 m in height (measurement height ~22 m) and the mean canopy height was ~10 m. The CIMS was situated on the topmost platform, facing north toward the forest. The temperatures inside the instrument enclosure and CIMS flow region were controlled, and the instrument was shielded from the elements by an insulated enclosure. An ultrasonic anemometer extending off the tower on the north side, longitudinally separated from the inlet ~0.8 m, measured the 3D wind components and the converted virtual temperature. A weather station comprised of several sensors monitored the relative humidity (RH, percent), air temperature (*T*, degrees Centigrade), barometric pressure (*P*, millibars), solar radiation (watts per square meter), wind speed (meters per second), and wind direction (0–360°).

CIMS Mixing Ratios. The ionization mechanism and details about calibration for each species are presented in *SI Appendix*. Briefly, compounds were measured through a high-flow fluoropolymer-coated glass inlet (~40 cm long, 3.1 cm ID, ~2,000 $L \cdot min^{-1}$). The analytical method, using reagent ion CF_3O^-, is specific toward the detection of acids, hydroperoxides, multifunctional nitrates, and other multifunctional species. The ionization mechanism is fluoride transfer for acidic analytes and cluster formation for other analytes. The absolute sensitivity and water vapor dependence of the ionization were calibrated for each species in the laboratory by quantitative techniques (spectroscopy, gravimetry, liquid chromatography, etc.), when calibration standards are available commercially or can be synthesized and purified (11 out of 16 compounds). The sensitivities were calculated by ab initio methods otherwise. High-frequency CIMS measurement of water vapor was calibrated by 1-Hz weather station measurements of RH, *T*, and *P* after application of a temperature correction to the ion signal. In-field calibrations were performed every 2 h with commercially available standards, and in-field zero backgrounds were measured every half hour, under dry and ambient RH conditions.

Flux Calculations. Data processing protocols, flux quality assessment and criteria, standard corrections, and CIMS-specific corrections are documented in detail in *SI Appendix*. We limit the fluxes presented here to a few ideal days from the campaign period, characterized by the following conditions: The turbulence (measured by the momentum flux) is well established, the data reproducibility is high, the spectral analysis shows expected behavior for sampling in the inertial subrange, and the energy balance closure at the surface (Fig. 2) is adequately met. Acceptable data generally correspond to measurement periods for which winds were northerly, with exclusively forest fetch. Mixing ratios and the vertical wind were measured at 8 Hz or faster. A time response correction was applied for HNO_3 (factor of 1.62) as described in *SI Appendix*, section 5, due the measured flux dampening caused by the time delay of this compound from interactions with instrument surfaces. Measurement uncertainties ($\pm 1\sigma$) are largest for species with lower mean concentrations during the daytime, such as MTNP, which has a dominant nighttime source. A short period of atypical nighttime convection was removed from the data for Julian day 165 due to the flux criteria discussed in *SI Appendix*, section 4. EC fluxes of other species commonly detected by CIMS (notably, SO_2, glycolaldehyde, and methyl hydroperoxide) were not calculated in this work because mixing ratios at this site were either too rapidly changing (SO_2 plumes) or contain interfering species when measured with the time-of-flight mass detector.

ACKNOWLEDGMENTS. We thank the organizers and committee members of the SOAS campaign: A. G. Carlton, A. H. Goldstein, J. L. Jimenez, R. W. Pinder, J. de Gouw, B. J. Turpin, and A. B. Guenther. We acknowledge C. J. Groff at Purdue University for his help with leaf area index measurements and tree surveys. We thank D. J. Jacob and the Atmospheric Chemistry Modeling Group at Harvard University for making GEOS–Chem available for this work. Meteorological data used in the GEOS–Chem simulations were provided by the Global Modeling and Assimilation Office at NASA Goddard Space Flight Center. We acknowledge funding from the National Science Foundation (NSF) under Grant AGS-1240604 and NSF Postdoctoral Research Fellowship program Award AGS-1331360. Financial and logistical support for SOAS was provided by the NSF, the Earth Observing Laboratory at the National Center for Atmospheric Research (operated by NSF), the personnel at Atmospheric Research and Analysis, and the Electric Power Research Institute.

1. Guenther A (2002) The contribution of reactive carbon emissions from vegetation to the carbon balance of terrestrial ecosystems. *Chemosphere* 49(8):837–844.
2. Carlton AG, Wiedinmyer C, Kroll JH (2009) A review of secondary organic aerosol formation from isoprene. *Atmos Chem Phys* 9(14):4987–5005.
3. Mao J, et al. (2013) Ozone and organic nitrates over the eastern United States: Sensitivity to isoprene chemistry. *J Geophys Res* 118(19):11,256–11,268.
4. Lelieveld J, et al. (2008) Atmospheric oxidation capacity sustained by a tropical forest. *Nature* 452(7188):737–740.
5. Xie Y, et al. (2013) Understanding the impact of recent advances in isoprene photooxidation on simulations of regional air quality. *Atmos Chem Phys* 13(16):8439–8455.
6. Paulot F, et al. (2011) Importance of secondary sources in the atmospheric budgets of formic and acetic acids. *Atmos Chem Phys* 11(5):1989–2013.
7. Horowitz LW, et al. (2007) Observational constraints on the chemistry of isoprene nitrates over the eastern United States. *J Geophys Res* 112(D12):D12S08.
8. Fowler D, Duyzer J, Andreae M, Schimel D (1989) *Micrometeorological Techniques for the Measurement of Trace Gas Exchange* (Wiley, New York).
9. Karl T, et al. (2004) Exchange processes of volatile organic compounds above a tropical rain forest: Implications for modeling tropospheric chemistry above dense vegetation. *J Geophys Res* 109(D18):D18306.
10. Park J-H, et al. (2013) Active atmosphere-ecosystem exchange of the vast majority of detected volatile organic compounds. *Science* 341(6146):643–647.
11. Bessagnet B, Seigneur C, Menut L (2010) Impact of dry deposition of semi-volatile organic compounds on secondary organic aerosols. *Atmos Environ* 44(14):1781–1787.
12. Ahmadov R, et al. (2012) A volatility basis set model for summertime secondary organic aerosols over the eastern United States in 2006. *J Geophys Res* 117(D6):D06301.
13. Knote C, Hodzic A, Jimenez JL (2014) The effect of dry and wet deposition of condensable vapors on secondary organic aerosols concentrations over the continental US. *Atmos Chem Phys Discuss* 14(9):13731–13767.
14. Zhang L, Brook J, Vet R (2003) A revised parameterization for gaseous dry deposition in air-quality models. *Atmos Chem Phys* 3(6):2067–2082.
15. Müller M, et al. (2010) First eddy covariance flux measurements by PTR-TOF. *Atmos Meas Tech* 3(2):387–395.
16. Baldocchi DD, Hincks BB, Meyers TP (1988) Measuring biosphere-atmosphere exchanges of biologically related gases with micrometeorological methods. *Ecology* 69 (5):1331–1340.
17. Crounse JD, McKinney KA, Kwan AJ, Wennberg PO (2006) Measurement of gas-phase hydroperoxides by chemical ionization mass spectrometry. *Anal Chem* 78(19): 6726–6732.
18. Kaminsky KZ, Dubayah R (1997) Estimation of surface net radiation in the boreal forest and northern prairie from shortwave flux measurements. *J Geophys Res* 102 (D24):29707–29716.
19. Oliphant A, et al. (2004) Heat storage and energy balance fluxes for a temperate deciduous forest. *Agric For Meteorol* 126(3):185–201.
20. Ganzeveld L, Valverde-Canossa J, Moortgat GK, Steinbrecher R (2006) Evaluation of peroxide exchanges over a coniferous forest in a single-column chemistry-climate model. *Atmos Environ* 40(0):68–80.
21. Munger JW, et al. (1996) Atmospheric deposition of reactive nitrogen oxides and ozone in a temperate deciduous forest and a subarctic woodland: 1. Measurements and mechanisms. *J Geophys Res* 101(D7):12639–12657.
22. Hall B, Claiborn C, Baldocchi D (1999) Measurement and modeling of the dry deposition of peroxides. *Atmos Environ* 33(4):577–589.
23. Hall BD, Claiborn CS (1997) Measurements of the dry deposition of peroxides to a Canadian boreal forest. *J Geophys Res* 102(D24):29343–29353.
24. Valverde-Canossa J, et al. (2006) First measurements of H_2O_2 and organic peroxides surface fluxes by the relaxed eddy-accumulation technique. *Atmos Environ* 40(Suppl 1):55–67.
25. Hartmann WR, Santana M, Hermoso M, Andreae MO, Sanhueza E (1991) Diurnal cycles of formic and acetic acids in the northern part of the Guayana shield, Venezuela. *J Atmos Chem* 13(1):63–72.
26. Kuhn U, et al. (2002) Exchange of short-chain monocarboxylic acids by vegetation at a remote tropical forest site in Amazonia. *J Geophys Res* 107(D20):8069.
27. Meyers T, Huebert B, Hicks B (1989) HNO_3 deposition to a deciduous forest. *Boundary Layer Metorol* 49(4):395–410.
28. Horii CV, et al. (2005) Atmospheric reactive nitrogen concentration and flux budgets at a Northeastern US forest site. *Agric For Meteorol* 133(1):210–225.
29. Farmer D, Wooldridge P, Cohen R (2006) Application of thermal-dissociation laser induced fluorescence (TD-LIF) to measurement of HNO_3, Σalkyl nitrates, Σperoxy nitrates, and NO_2 fluxes using eddy covariance. *Atmos Chem Phys* 6(11):3471–3486.
30. Farmer D, Cohen R (2008) Observations of HNO_3, ΣAN, ΣPN and NO_2 fluxes: Evidence for rapid HO_x chemistry within a pine forest canopy. *Atmos Chem Phys* 8(14):3899–3917.
31. Lee X, Massman W, Law BE (2006) *Handbook of Micrometeorology: A Guide for Surface Flux Measurement and Analysis* (Springer, New York).
32. Jensen NO, Hummelshøj P (1995) Derivation of canopy resistance for water vapour fluxes over a spruce forest, using a new technique for the viscous sublayer resistance. *Agric For Meteorol* 73(3-4):339–352.
33. Jensen NO, Hummelshøj P (1997) Erratum to Derivation of canopy resistance for water vapour fluxes over a spruce forest, using a new technique for the viscous sublayer resistance. *Agric For Meteorol* 85(3):289.
34. Wesely M, Hicks B (2000) A review of the current status of knowledge on dry deposition. *Atmos Environ* 34(12):2261–2282.
35. Wesely ML (1989) Parameterization of surface resistances to gaseous dry deposition in regional-scale numerical models. *Atmos Environ* 23(6):1293–1304.
36. Kampf CJ, et al. (2013) Effective Henry's law partitioning and the salting constant of glyoxal in aerosols containing sulfate. *Environ Sci Technol* 47(9):4236–4244.
37. Ip HSS, Huang XHH, Yu JZ (2009) Effective Henry's law constants of glyoxal, glyoxylic acid, and glycolic acid. *Geophys Res Lett* 36(1):L01802.
38. Snedden WA, Chung I, Pauls RH, Bown AW (1992) Proton/l-glutamate symport and the regulation of intracellular pH in isolated mesophyll cells. *Plant Physiol* 99(2): 665–671.
39. Van Hove LWA, Adema EH, Vredenberg WJ, Pieters GA (1989) A study of the adsorption of NH_3 and SO_2 on leaf surfaces. *Atmos Environ* 23(7):1479–1486.
40. Sander R (1999) *Compilation of Henry's Law Constants for Inorganic and Organic Species of Potential Importance in Environmental Chemistry* (Max Planck Inst Chem, Mainz, Germany).
41. Stavrakou T, et al. (2012) Satellite evidence for a large source of formic acid from boreal and tropical forests. *Nat Geosci* 5(1):26–30.
42. Bates KH, et al. (2014) Gas phase production and loss of isoprene epoxydiols. *J Phys Chem A* 118(7):1237–1246.
43. Neeb P, Sauer F, Horie O, Moortgat GK (1997) Formation of hydroxymethyl hydroperoxide and formic acid in alkene ozonolysis in the presence of water vapor. *Atmos Environ* 31(15):1417–1423.
44. Marklund S (1971) The simultaneous determination of bis(hydroxymethyl)peroxide (BHMP), hydroxymethylhydroperoxide (HMP), and H_2O_2 with Titanium (IV). Equilibria between peroxides and stabilities of HMP and BHMP at physiological conditions. *Acta Chem Scand* 25(9):3517–3531.
45. Goldstein AH, et al. (2004) Forest thinning experiment confirms ozone deposition to forest canopy is dominated by reaction with biogenic VOCs. *Geophys Res Lett* 31(22): L22106.
46. Hewitt CN, Kok GL, Fall R (1990) Hydroperoxides in plants exposed to ozone mediate air pollution damage to alkene emitters. *Nature* 344(6261):56–58.
47. Fares S, Loreto F, Kleist E, Wildt J (2008) Stomatal uptake and stomatal deposition of ozone in isoprene and monoterpene emitting plants. *Plant Biol (Stuttg)* 10(1):44–54.
48. Jardine K, et al. (2011) Within-canopy sesquiterpene ozonolysis in Amazonia. *J Geophys Res* 116(D19):D19301.
49. Zhang L, et al. (2012) Nitrogen deposition to the United States: Distribution, sources, and processes. *Atmos Chem Phys* 12(10):4539–4554.
50. Allen NDC, González Abad G, Bernath PF, Boone CD (2013) Satellite observations of the global distribution of hydrogen peroxide (H_2O_2) from ACE. *J. Quant. Spectrosc Radiat Transfer* 115:66–77.
51. Mao J, et al. (2010) Chemistry of hydrogen oxide radicals (HO_x) in the Arctic troposphere in spring. *Atmos Chem Phys* 10(13):5823–5838.
52. Li Q, et al. (2000) Atmospheric hydrogen cyanide (HCN): Biomass burning source, ocean sink? *Geophys Res Lett* 27(3):357–360.

53. Bey I, et al. (2001) Global modeling of tropospheric chemistry with assimilated meteorology: Model description and evaluation. *J Geophys Res* 106(D19):23073–23095.
54. Lee L, Teng AP, Wennberg PO, Crounse JD, Cohen RC (2014) On rates and mechanisms of OH and O_3 reactions with isoprene-derived hydroxy nitrates. *J Phys Chem A* 118(9): 1622–1637.
55. Lee M, Heikes BG, O'Sullivan DW (2000) Hydrogen peroxide and organic hydroperoxide in the troposphere: A review. *Atmos Environ* 34(21):3475–3494.
56. Crounse JD, Paulot F, Kjaergaard HG, Wennberg PO (2011) Peroxy radical isomerization in the oxidation of isoprene. *Phys Chem Chem Phys* 13(30):13607–13613.
57. Paulot F, Henze DK, Wennberg PO (2012) Impact of the isoprene photochemical cascade on tropical ozone. *Atmos Chem Phys* 12(3):1307–1325.
58. Tie X, et al. (2003) Effect of clouds on photolysis and oxidants in the troposphere. *J Geophys Res* 108(D20):4642.
59. Sander SP, et al. (2006) *Chemical Kinetics and Photochemical Data for Use in Stratospheric Modeling: Evaluation Number 15* (Jet Propulsion Lab, Pasadena, CA) JPL Publ 06-2.
60. Bauerle S, Moortgat GK (1999) Absorption cross-sections of $HOCH_2OOH$ vapor between 205 and 360 nm at 298 K. *Chem Phys Lett* 309(1-2):43–48.
61. Orlando JJ, Tyndall GS (2003) Gas phase UV absorption spectra for peracetic acid, and for acetic acid monomers and dimers. *J Photochem Photobiol Chem* 157(2-3):161–166.
62. Gaston CJ, et al. (2014) Reactive uptake of an isoprene-derived epoxydiol to submicron aerosol particles. *Environ Sci Technol* 48(19):11178–11186.
63. Müller J-F, Peeters J, Stavrakou T (2014) Fast photolysis of carbonyl nitrates from isoprene. *Atmos Chem Phys* 14(5):2497–2508.
64. Carlton AG, Turpin BJ (2013) Particle partitioning potential of organic compounds is highest in the Eastern US and driven by anthropogenic water. *Atmos Chem Phys* 13(20):10203–10214.
65. Lin Y-H, et al. (2012) Isoprene epoxydiols as precursors to secondary organic aerosol formation: Acid-catalyzed reactive uptake studies with authentic compounds. *Environ Sci Technol* 46(1):250–258.
66. Eddingsaas NC, VanderVelde DG, Wennberg PO (2010) Kinetics and products of the acid-catalyzed ring-opening of atmospherically relevant butyl epoxy alcohols. *J Phys Chem A* 114(31):8106–8113.
67. Lin YH, Knipping EM, Edgerton ES, Shaw SL, Surratt JD (2013) Investigating the influences of SO_2 and NH_3 levels on isoprene-derived secondary organic aerosol formation using conditional sampling approaches. *Atmos Chem Phys* 13(16):8457–8470.
68. Lin Y-H, et al. (2014) Light-absorbing oligomer formation in secondary organic aerosol from reactive uptake of isoprene epoxydiols. *Environ Sci Technol* 48(20): 12012–12021.
69. Nguyen TB, et al. (2014) Organic aerosol formation from the reactive uptake of isoprene epoxydiols (IEPOX) onto non-acidified inorganic seeds. *Atmos Chem Phys* 14(7): 3497–3510.
70. Bryan A, et al. (2012) In-canopy gas-phase chemistry during CABINEX 2009: Sensitivity of a 1-D canopy model to vertical mixing and isoprene chemistry. *Atmos Chem Phys* 12(18):8829–8849.
71. Steiner A, et al. (2011) Analysis of coherent structures and atmosphere-canopy coupling strength during the CABINEX field campaign. *Atmos Chem Phys* 11(23): 11921–11936.
72. Guenther A, et al. (1996) Estimates of regional natural volatile organic compound fluxes from enclosure and ambient measurements. *J Geophys Res* 101(D1):1345–1359.
73. Crounse JD, Nielsen LB, Jørgensen S, Kjaergaard HG, Wennberg PO (2013) Autoxidation of organic compounds in the atmosphere. *J Phys Chem Lett* 4(20):3513–3520.
74. Sandermann H, Jr (1996) Ozone and plant health. *Annu Rev Phytopathol* 34(1): 347–366.
75. Sandermann H, Jr, Ernst D, Heller W, Langebartels C (1998) Ozone: An abiotic elicitor of plant defence reactions. *Trends Plant Sci* 3(2):47–50.
76. Mehlhorn H (1990) Ethylene-promoted ascorbate peroxidase activity protects plants against hydrogen peroxide, ozone and paraquat. *Plant Cell Environ* 13(9):971–976.
77. Finkelstein PL, et al. (2000) Ozone and sulfur dioxide dry deposition to forests: Observations and model evaluation. *J Geophys Res* 105(D12):15365–15377.
78. Rummel U, et al. (2007) Seasonal variation of ozone deposition to a tropical rain forest in southwest Amazonia. *Atmos Chem Phys* 7(20):5415–5435.
79. Yan J, Tsuichihara N, Etoh T, Iwai S (2007) Reactive oxygen species and nitric oxide are involved in ABA inhibition of stomatal opening. *Plant Cell Environ* 30(10):1320–1325.
80. Lum HK, Butt YK, Lo SC (2002) Hydrogen peroxide induces a rapid production of nitric oxide in mung bean (*Phaseolus aureus*). *Nitric Oxide* 6(2):205–213.
81. Lind JA, Lazrus AL, Kok GL (1987) Aqueous phase oxidation of sulfur (IV) by hydrogen peroxide, methylhydroperoxide, and peroxyacetic acid. *J Geophys Res* 92(D4): 4171–4177.
82. Fenton H (1894) Oxidation of tartaric acid in presence of iron. *J Chem Soc Trans* 65: 899–910.
83. Lovett GM, Lindberg SE (1993) Atmospheric deposition and canopy interactions of nitrogen in forests. *Can J For Res* 23(8):1603–1616.
84. Wolfe GM, et al. (2009) Eddy covariance fluxes of acyl peroxy nitrates (PAN, PPN and MPAN) above a Ponderosa pine forest. *Atmos Chem Phys* 9(2):615–634.
85. Neff J, Holland E, Dentener F, McDowell W, Russell K (2002) The origin, composition and rates of organic nitrogen deposition: A missing piece of the nitrogen cycle? *Biogeochemistry* 57-58(1):99–136.
86. Lockwood AL, Filley TR, Rhodes D, Shepson PB (2008) Foliar uptake of atmospheric organic nitrates. *Geophys Res Lett* 35(15):L15809.
87. Sparks JP, Roberts JM, Monson RK (2003) The uptake of gaseous organic nitrogen by leaves: A significant global nitrogen transfer process. *Geophys Res Lett* 30(23):2189.
88. Paulot F, et al. (2009) Unexpected epoxide formation in the gas-phase photooxidation of isoprene. *Science* 325(5941):730–733.
89. Jacobs MI, Darer AI, Elrod MJ (2013) Rate constants and products of the OH reaction with isoprene-derived epoxides. *Environ Sci Technol* 47(22):12868–12876.
90. Paulot F, et al. (2009) Isoprene photooxidation: New insights into the production of acids and organic nitrates. *Atmos Chem Phys* 9(4):1479–1501.
91. Jacobs MI, Burke WJ, Elrod MJ (2014) Kinetics of the reactions of isoprene-derived hydroxynitrates: Gas phase epoxide formation and solution phase hydrolysis. *Atmos Chem Phys Discuss* 14(8):12121–12165.
92. Peeters J, Nguyen TL, Vereecken L (2009) HO_x radical regeneration in the oxidation of isoprene. *Phys Chem Chem Phys* 11(28):5935–5939.
93. Beaver MR, et al. (2012) Importance of biogenic precursors to the budget of organic nitrates: Observations of multifunctional organic nitrates by CIMS and TD-LIF during BEARPEX 2009. *Atmos Chem Phys* 12(13):5773–5785.
94. Tyndall GS, et al. (2001) Atmospheric chemistry of small organic peroxy radicals. *J Geophys Res* 106(D11):12157–12182.